

# The origin of platinum group minerals in oceanic crust

Katy Evans<sup>1,\*</sup>, Steven M. Reddy<sup>1</sup>, Renaud Merle<sup>2</sup>, Denis Fougereuse<sup>1</sup>, William D.A. Rickard<sup>3</sup>, David W. Saxey<sup>3</sup>, Jung-Woo Park<sup>4</sup>, Luc Doucet<sup>1</sup>, and Fred Jourdan<sup>1</sup>

<sup>1</sup>School of Earth and Planetary Sciences, Curtin University, GPO Box U1985, Perth, WA 6845, Australia

<sup>2</sup>Department of Earth Sciences, Uppsala University, 752 36 Uppsala, Sweden

<sup>3</sup>John de Laeter Centre, Curtin University, GPO Box U1985, Perth, WA 6845, Australia

<sup>4</sup>School of Earth and Environmental Sciences, Seoul National University, Seoul 08826, South Korea

## ABSTRACT

Highly siderophile elements (HSEs), including Re and Os, are used extensively as geochemical tracers and geochronometers to investigate the formation and evolution of Earth's crust and mantle. Mantle rocks are commonly serpentinized, but the effect of serpentinization on the distribution of HSEs is controversial because HSEs are commonly hosted by rare, micrometer-to sub-micrometer-scale grains of platinum group minerals (PGMs) of ambiguous origin that are challenging to identify, characterize, and interpret. In this study, atom probe tomography (APT) is used to characterize two spatially close PGM grains hosted by a partially serpentinized harzburgite from Macquarie Island, Australia. The APT data reveal an extraordinary level of detail that provides insights into the origin of a complex Cu–Pt alloy grain (average composition ~Cu<sub>4</sub>Pt). The grain hosts Fe-, Ni-, and Pt-rich sub-grains associated with Rh, variably overlapping networks of Pd- and Cd-enrichment, and OH-rich volumes identified as fluid inclusions. Osmium and Ru are hosted by an idioblastic laurite (RuS<sub>2</sub>) grain. Compositional, textural, and phase-diagram constraints are consistent with a modified pre-serpentinization origin for the PGMs, and a comparison between observed and calculated grain distributions indicate that while Os isotope ratios were probably unaffected by serpentinization, whole-rock and grain-scale HSE and isotopic ratios may have been decoupled during serpentinization.

## INTRODUCTION

Highly siderophile elements (HSEs), including Re and Os, are hosted dominantly by non-silicate sulfide minerals and metallic alloys. They provide a unique and valuable complement to elements that record changes to silicate mineral assemblages and melts and are used extensively to interrogate Earth systems (e.g., Day et al., 2016). Further, the HSEs are variably compatible during mantle melting, so the HSE characteristics of peridotites provide a sensitive record of the evolution of Earth's mantle and the processes that drove that evolution (e.g., Luguet and Reisberg, 2016).

However, mantle peridotites are commonly partially or extensively serpentinized. Mantle rocks are highly reactive in the presence of water, and most accessible peridotites have been exposed to either seawater or crustal flu-

ids (Becker and Dale, 2016). Conditions during serpentinization can be sufficiently reducing that primary sulfide minerals such as pentlandite (Fe,Ni)<sub>9</sub>S<sub>8</sub> are destabilized in favor of secondary minerals such as heazlewoodite (Ni<sub>3</sub>S<sub>2</sub>), alloy phases such as awaruite (Ni<sub>3</sub>Fe), and platinum group minerals (PGMs), including alloys (e.g., Zhu and Zhu, 2019). The effect of serpentinization on the distribution of HSEs and the Re–Os system is controversial. Commonly, it is assumed that <sup>187</sup>Os/<sup>188</sup>Os ratios are unaffected by serpentinization (e.g., Rudnick and Walker, 2009; Secchiari et al., 2020; Zhang, 2008). But there is growing evidence that HSEs, including Re and Os, are mobilized by serpentinization (Beinlich et al., 2020; Cabri et al., 2022; Gorman et al., 2019; Jiménez-Franco et al., 2020; Keays et al., 2021), with implications for the interpretation of HSE and Os isotope data (Foustoukos, 2019).

To constrain HSE mobility during serpentinization, it is necessary to understand the origins of PGMs in serpentinites. Proposed origins for ser-


pentinite-hosted PGMs include formation within Earth's core during ancient depletion events, formation within the mantle during melting or refertilization, serpentinization, and weathering (Aiglsperger et al., 2016; Cabri et al., 2022; Garuti et al., 2012; Keays et al., 2021; Lawley et al., 2020; Parman et al., 2015; Wainwright et al., 2015). This diversity reflects challenges inherent in characterization of these phases, which are typically rare and tiny (Foustoukos et al., 2015). Fortunately, atom probe tomography (APT), a relatively new technique in the Earth sciences (Reddy et al., 2020), permits atom-scale reconstruction of the compositions of alloy grains (Parman et al., 2015). Here, we derive insights into the origins and mobility of HSEs during serpentinization via nanometer-scale APT analysis of an alloy grain from Macquarie Island, Australia.

## GEOLOGICAL SETTING

Peridotite samples were collected from the Boot Hill locality, Macquarie Island, Australia (Figs. 1A and 1B). Macquarie Island exposes oceanic crust uplifted, without obduction, by intra-oceanic faulting and presents an ideal opportunity for investigating serpentinization that occurred on or below the ocean floor. Details of the locality and its geological history are provided by Dijkstra et al. (2010). Typical outcrops are a few square meters in size and comprise partially serpentinized layers of dunite and harzburgite (e.g., Fig. 1C). Sample MQ17-16 (section C3L-033: 57F 494673 mE 3958499 mN relative to the WGS84 datum) is a heterogeneously serpentinized harzburgite from an outcrop that also hosts dunite channels (Figs. 1C and 1D).

## METHODS

Detailed methods are provided in the Supplemental Material<sup>1</sup>. Five thin sections from each

Katy Evans  <https://orcid.org/0000-0001-5144-4507>

\*k.evans@curtin.edu.au

<sup>1</sup>Supplemental Material. Methods and petrographic description. Please visit <https://doi.org/10.1130/GEOL.S.22304566> to access the supplemental material, and contact [editing@geosociety.org](mailto:editing@geosociety.org) with any questions.

CITATION: Evans, K., et al., 2023, The origin of platinum group minerals in oceanic crust: *Geology*, v. 51, p. 554–558, <https://doi.org/10.1130/G50927.1>

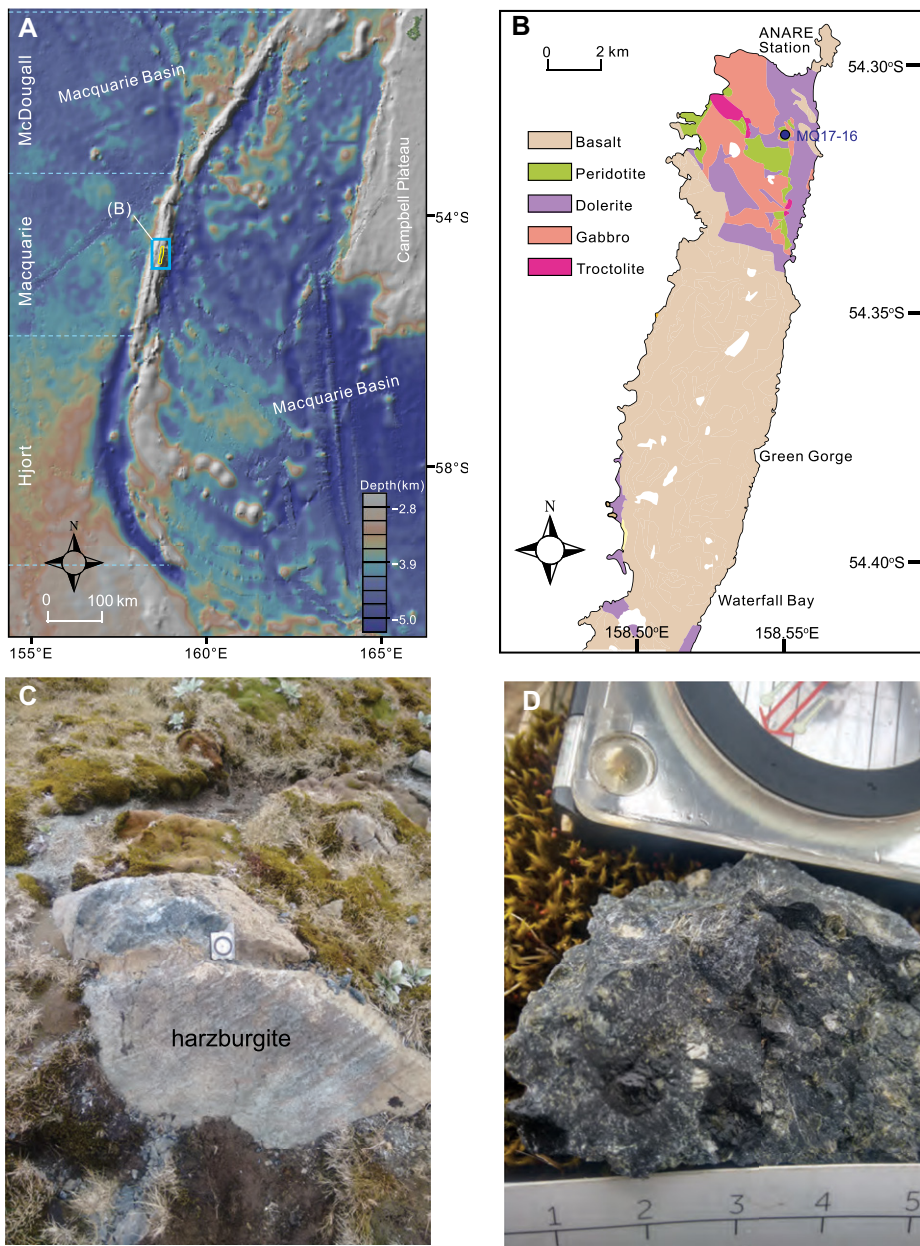


**Figure 1.** (A) Regional bathymetric map showing Macquarie Island, Australia. Hjort, Macquarie, McDougall refer to different sections of the plate boundary. (B) Geological map of northern and central parts of Macquarie Island showing Boot Hill sample locality. ANARE—Australian National Antarctic Research Expeditions station. (C) Harzburgite outcrop with dunite channel sampled to acquire sample MQ17-16. (D) Sample MQ17-16.

sample were characterized by reflected and transmitted light microscopy. PGM grains were identified using an automated mapping routine on a TESCAN TIMA scanning electron microscope (SEM). Bulk rock concentrations of platinum group elements (PGEs) were analyzed by the Ni-sulfide fire assay–isotope dilution inductively coupled plasma mass spectrometry (ICP-MS) method of Park et al. (2012), and Re and Os isotope ratios were measured by isotope dilution thermal ionization mass spectrometry (TIMS) using a TritonTM multicollector instrument. Needle-shaped specimens, a few micrometers long, were prepared in a TESCAN Lyra3 Ga<sup>+</sup>

focused ion beam SEM (FIB-SEM) following Rickard et al. (2020). APT data were collected on a Cameca LEAP 4000X HR and ranged and reconstructed in three dimensions using Cameca's APSuite 6 proprietary software.

## RESULTS

Serpentinized olivine and orthopyroxene form islands within a texturally complex serpentine matrix (Fig. S1 in the Supplemental Material). Serpentine textures are consistent with the presence of lizardite after olivine, chrysotile within veins, and an absence of antigorite. Early and late trace sulfides include heazle-

woodite, pentlandite, and cobaltian pentlandite. Awaruite occurs within magnetite-bearing serpentine veins and associated with a composite heazlewoodite–magnetite grain that overprints late tremolite. Further petrographic details are provided in the Supplemental Material.

Automated mapping revealed inclusions of laurite (RuS<sub>2</sub>) and a Cu–Pt alloy phase within a composite heazlewoodite–pentlandite–cobaltian pentlandite–magnetite grain, 20 × 30 μm in size, that is located on the margin of an altered orthopyroxene grain within the serpentine matrix (Fig. 2A). This grain comprises irregular to angular sulfide sub-grains patchily enriched in Co, Cu, and Ni within a boxwork of magnetite or iron oxides. The PGMs include a semi-circular Cu–Pt alloy grain, 5 μm across, on the margin of heazlewoodite and an idioblastic laurite inclusion, 2 μm across, within the same grain (Fig. 2A).

Bulk-rock PGE patterns are relatively flat and are enriched relative to primitive mantle, except for Re and Au (Table S1 in the Supplemental Material; Fig. 2B). The <sup>187</sup>Re/<sup>188</sup>Os ratio is 0.012, the <sup>187</sup>Os/<sup>188</sup>Os ratio is 0.12569, the Re-depletion model age (T<sub>RD</sub>) is ca. 537 Ma, and the model age for separation from a chondritic mantle reservoir (T<sub>MA</sub>) is ca. 552 Ma (Table S2).

Five atom-probe needles were extracted: three from the alloy phase, and two from laurite (Fig. 2A). During APT analysis, alloy needles ran for as long as 20 h and produced as much as 100 million atoms. The laurite specimens fractured during initial setup of the atom probe analysis and only preliminary data were acquired. However, these data are sufficient to show that Os, Ir, and Ru are hosted by laurite (Fig. S2).

The alloy needles are heterogeneous and complex (Fig. 3). The matrix of the alloy comprises mainly Cu and Pt (Cu + Pt = 94.3 at%) with Fe, Ni, and Pd (Cu + Pt + Fe + Pd + Ni = 99.3 at%; Table S3). Curved planar interfaces defined by the segregation of Cd and Pd form a three-dimensional network of grain boundaries within the alloy (i, Fig. 3). Pd is also locally enriched at the center of sub-grains (ii, Fig. 3), and Pd is not associated with other HSEs.

Along some parts of the grain-boundary interfaces, enrichments of Pt, Rh, Fe, and Ni define irregular, variably elongate, 50–200-nm-long sub-grains with variable aspect ratios that extend along the grain boundary network and are interpreted as separate phases (iii, Fig. 3). These sub-grains show some evidence of zoning, with Fe (red surface in Fig. 3 delineates 7 at% Fe) concentrated toward the center of the sub-grains, and Ni (green) and Rh (lavender) enriched toward their margins (Fig. 3). Copper (not shown) is relatively homogeneously distributed within the alloy. In contrast, Pt (not shown) occurs throughout the matrix but is more concentrated within the Fe- and Ni-rich sub-grains (Table S3).

Volumes, a few tens of nanometers in size, are enriched in OH<sub>3</sub> (pink, iv, Fig. 3). The

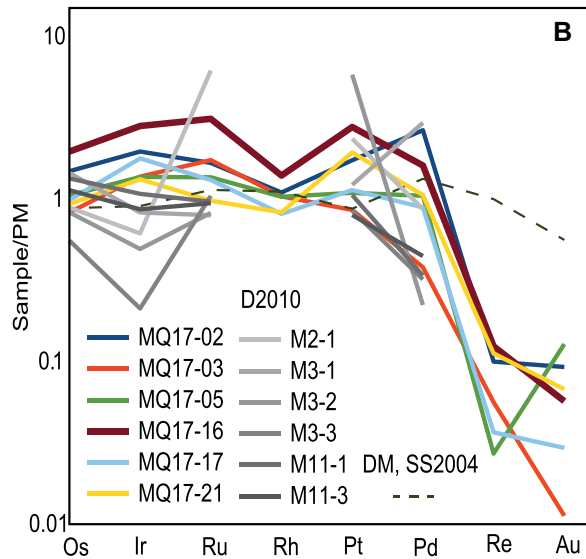
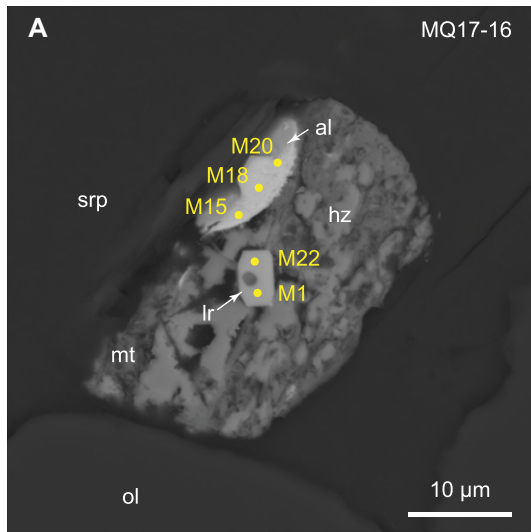


**Figure 2. (A)** Altered heazlewoodite grain showing alloy and laurite inclusions discussed in text and locations of needles sampled for atom probe tomography. Labels refer to needle ID. **(B)** Platinum group element + Re + Au concentrations for Boot Hill peridotites normalized to primitive mantle (PM) (McDonough and Sun, 1995). al—alloy; hz—heazlewoodite; Ir—laurite; mt—magnetite; ol—olivine; srp—serpentine; SS—Salters and Stracke (2004); DM—depleted mantle; D10—Dijkstra et al. (2010).

morphology of these volumes indicates rapid evaporation and is consistent with features produced by fluid inclusions (Dubosq et al., 2020; Reddy et al., 2020). These inclusions lie on the Cd-enriched networks that connect the Fe-, Ni-, and Pt-enriched sub-grains.

## DISCUSSION

### Host Rock Characteristics

The PGE patterns,  $^{187}\text{Re}/^{188}\text{Os}$  ratio,  $^{187}\text{Os}/^{188}\text{Os}$  ratio, and anhydrous mineral assemblage are consistent with the descriptions of peridotites from the same locality by Dijkstra et al. (2010), who used major, trace, rare earth, and HSE element patterns to infer that the highly

depleted peridotites were modified by melt-rock reaction during the Miocene.

### Textural Constraints

The nanometer-scale heterogeneity of the alloy is not diagnostic of its origin; nanometric to micrometric base-metal sulfides and PGMs described by Luguet and Pearson (2019) show complexity and heterogeneity in  $^{187}\text{Os}/^{188}\text{Os}$  and  $^{187}\text{Re}/^{188}\text{Os}$  values that are attributed to differences between residual and metasomatic grains and Re-Os fractionation related to transport, precipitation, and melt-rock reaction within the mantle lithosphere. However, the inclusion of the PGMs within heazlewoodite, which forms by desulfidation during early serpentinization,

indicates that they formed prior to late serpentinization.

Complex Pt- and Cu-bearing secondary alloys form during serpentinization (Augé et al., 1999; Cabri et al., 2022). Porous tomamaeite ( $\text{Cu}_3\text{Pt}$ ), interpreted to have formed during serpentinization, forms an inclusion within a native Os grain from alluvial river sediments of the southern Urals, Russia (Sharygin and Mikhaiov, 2022). The porosity of the tomamaeite indicates a secondary origin, in contrast to the non-porous Cu–Pt grain from sample MQ17-16 (Figs. 2A and 3). Tulameenite ( $\text{Pt}_2\text{CuFe}$ ) is a Pt–Cu–Fe mineral formed by serpentinization (Cabri and Genkin, 1991), but its composition does not match that of the bulk alloy, the matrix, or the sub-grains of sample MQ17-16 (Table S3).

Laurite can form by melt-rock reaction within the mantle or during hydrothermal alteration, including serpentinization (Ahmed and Bevan, 1981; Foustoukos et al., 2015). Laurite grains formed under hydrothermal conditions are typically subhedral to anhedral, zoned, and tens of micrometers in size (Zaccarini and Garuti, 2020), contrasting with the small, unzoned, euhedral grain within sample MQ17-16, which is more consistent with formation within the mantle.

### Phase Diagram Constraints and Network Formation

Cu–Pt alloys undergo phase transitions as temperature decreases from  $\sim 650$  to  $350$  °C (Abe et al., 2006; Matsumoto et al., 1996; Fig. 4A). The observed Cu:Pt ratios (e.g., iii, Fig. 3) are consistent with cooling-driven sub-grain formation from an originally homogeneous grain that formed above the temperature of serpentine stability ( $>650$  °C) (Fig. 4A). Iron and Ni are compatible with Pt, and this may have contributed to the formation of the Fe-, Ni-, and Pt-rich sub-grains. The binary phase

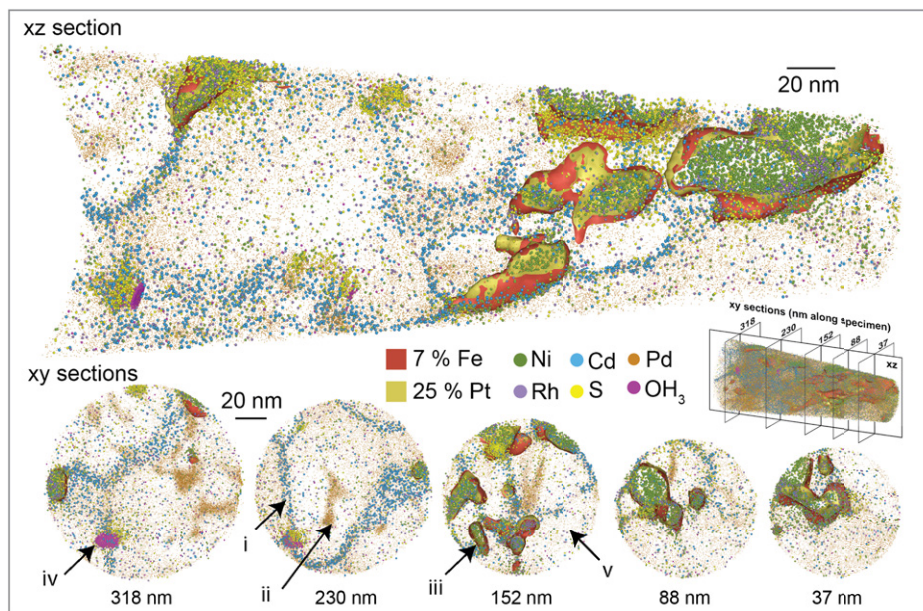


**Figure 3. Reconstruction of atom probe data for needle M20 showing distributions of elements discussed in text. Dot size varies to optimize clarity, and Cu and Pt atoms are not shown for same reason. Labels i to v indicate features mentioned in text.**

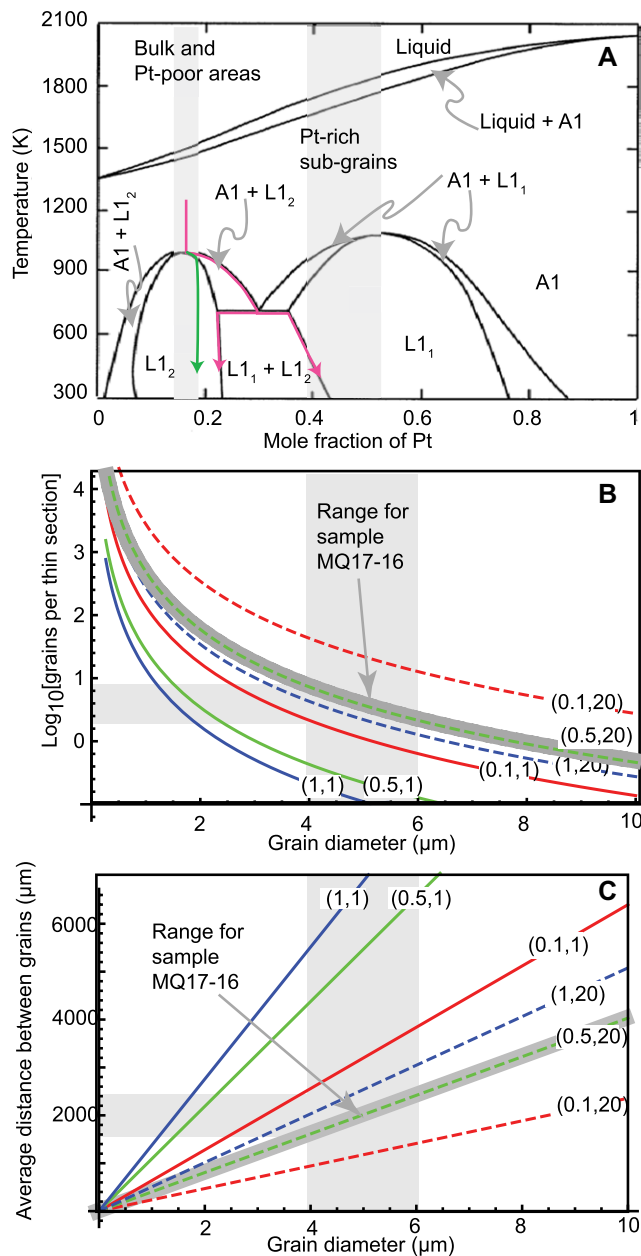


**Figure 4. (A) Cu–Pt phase diagram after Abe et al. (2006) showing formation of Pt-rich (pink) and Pt-poor (green) regions from precursor A1 grain. A1: disordered face centered cubic phase; L<sub>1</sub>, L<sub>2</sub>: ordered phase. (B) Number of grains per thin section versus grain diameter. Values in parentheses are mass fraction of platinum group elements (PGEs) in platinum group minerals (PGMs) (0.1, 0.5, or 1) and bulk rock PGE content (1 or 20 ppb), respectively. (C) Calculated distance between PGM grains as a function of grain diameter. Values in brackets as for B. Horizontal and gray bars show best estimates for sample MQ17-16.**

diagram does not account for the effects of the ~5% of the alloy that is not Cu or Pt. Minor and trace elements may migrate onto internal grain boundaries with decreasing temperature and extent of solid solution (e.g., Tacchetto et al., 2021); this process may have contributed to formation of the Pd-rich network and Fe- and Pt-rich sub-grains.

### Modification by Serpentinization

The OH<sub>3</sub> clusters, which are interpreted as fluid inclusions, provide strong support for grain formation or modification in the presence of aqueous fluid, and the presence of lizardite and chrysotile are consistent with serpentinization below the temperature of antigorite stability (<300 °C; Evans, 2004). The relationship of the OH<sub>3</sub> clusters to the Pd- and Cd-rich networks is

consistent with entrapment of secondary fluid inclusions on sub-grain boundaries in a water-bearing environment. Pd is unusual amongst the PGEs in that it is mobile during hydrothermal alteration (Becker and Dale, 2016; Cabri et al., 2022) and can form complexes with Cl, consistent with addition of externally derived Pd. However, the sub-grain interiors are also enriched in Pd, so some of the Pd on the networks may have migrated onto the grain boundaries from the sub-grain interiors. Further work is necessary to constrain the contributions of the two sources and the origin of the Cd, which are unclear.

### Environment of Formation

The geodynamic setting and some textural evidence are consistent with either a mantle or a serpentinization-related origin for the PGMs.

However, the phase diagram and morphology of the PGMs are more consistent with formation at >650 °C prior to serpentinization, followed by exsolution, sub-grain formation, and formation of the trace element-enriched networks within the alloy grain during re-equilibration with decreasing temperature. Fluid inclusions unambiguously record modification within a hydrous environment. Integrating these observations, we infer that the laurite and Cu–Pt alloy formed within the mantle prior to serpentinization but were modified during serpentinization to form the fluid inclusions, sub-grain structure, and the Pd- and Cd-enriched networks. The enclosing heazlewoodite would have protected the PGMs from later alteration.

### Implications for the Re–Os System and the Distribution of HSEs

The consequences of PGM modification for HSEs and the Re–Os system depend on the length scales of HSE transport and equilibration. The expected number of PGM grains per thin section and the average separation were calculated as a function of grain and bulk rock PGE contents and PGM grain diameter (Figs. 4B and 4C; see the Supplemental Material for details). The number and size of PGM grains in sample MQ17-16 is consistent with predictions based on bulk rock values, indicating that transport on length scales longer than that of the hand specimen is not required to explain the PGM mineral distribution (Fig. 4B). If the PGMs formed during serpentinization, then transport of HSEs is implied because the size of the grains requires collection of HSEs from a rock volume with a radius much larger (~2000 μm; Fig. 4C) than the distance between the alloy and laurite grains (a few micrometers). However, if, as seems more likely, the PGMs formed prior to serpentinization, then HSE mobility during serpentinization is not required to explain the bulk rock data. Nevertheless, intra-grain HSE mobility during serpentinization is recorded by redistribution of HSEs within the alloy grain (Fig. 3). If this mobility extends beyond the grain boundary, then serpentinization may decouple whole-rock and grain-scale HSE and isotopic ratios.

In summary, previously unseen complexity within serpentinite-hosted alloy grains revealed by APT records a multi-stage history extending from high-temperature mantle processes to low-temperature serpentinization. This and the mass balance calculations imply intra-grain micrometer-scale HSE mobility during serpentinization and decoupling between whole-rock and grain scale HSE distributions, with implications for the formation and alteration of PGMs in high- and low-temperature environments.

### ACKNOWLEDGMENTS

Reddy and Evans acknowledge support from TiGeR (The Institute of Geoscience Research) at Curtin

University and Australian Research Council Discovery grants DP210101866 and DP210102625. Whole-rock PGE analyses were funded by a Mid-Career Researcher Program (2022R1A2C1011741) through the National Research Foundation of Korea funded by the Ministry of Science and ICT, South Korea. Evans, Merle, and Jourdan acknowledge field-work support provided by the Australian Antarctic Division, Project 4444. A. Turbett, M. Raymond, L. Cabris, C. Lawley, and M. Bizimis are thanked for constructive reviews.

## REFERENCES CITED

- Abe, T., Sundman, B., and Onodera, H., 2006, Thermodynamic assessment of the Cu-Pt system: Journal of Phase Equilibria and Diffusion, v. 27, p. 5–13, <https://doi.org/10.1361/105497196X92736>.
- Ahmed, Z., and Bevan, J.C., 1981, Awaruite, iridian awaruite, and a new Ru-Os-Ir-Ni-Fe alloy from the Sakhakot-Qila complex, Malakand Agency, Pakistan: Mineralogical Magazine, v. 44, p. 225–230, <https://doi.org/10.1180/minmag.1981.044.334.17>.
- Aiglsperger, T., Proenza, J.A., Longo, F., Font-Bardia, M., Gali, S., Roqué, J., and Baurier-Aymat, S., 2016, Fibrous platinum-group minerals in “floating chromitites” from the Loma Larga Ni-laterite deposit, Dominican Republic: Minerals (Basel), v. 6, 126, <https://doi.org/10.3390/min6040126>.
- Augé, T., Cabri, L.J., Legendre, O., McMahon, G., and Cocherie, A., 1999, PGE distribution in base-metal alloys and sulfides of the New Caledonia ophiolite: Canadian Mineralogist, v. 37, p. 1147–1161.
- Becker, H., and Dale, C.W., 2016, Re-Pt-Os isotopic and highly siderophile element behavior in oceanic and continental mantle tectonites, in Harvey, J., and Day, J.M.D., eds., Highly Siderophile and Strongly Chalcophile Elements in High-Temperature Geochemistry and Cosmochemistry: Mineralogical Society of America Reviews in Mineralogy & Geochemistry 81, p. 369–440, <https://doi.org/10.1515/9781501502095-009>.
- Beinlich, A., von Heydebrand, A., Klemm, R., Martin, L., and Hicks, J., 2020, Desulphurisation, chromite alteration, and bulk rock PGE redistribution in massive chromitite due to hydrothermal overprint of the Pantan Intrusion, east Kimberley, Western Australia: Ore Geology Reviews, v. 118, <https://doi.org/10.1016/j.oregeorev.2019.103288>.
- Cabri, L.J., and Genkin, A.D., 1991, Re-examination of Pt alloys from lode and placer deposits, Urals: Canadian Mineralogist, v. 29, p. 419–425.
- Cabri, L.J., Oberthür, T., and Keays, R.R., 2022, Origin and depositional history of platinum-group minerals in placers—A critical review of facts and fiction: Ore Geology Reviews, v. 144, <https://doi.org/10.1016/j.oregeorev.2022.104733>.
- Day, J.M.D., Brandon, A.D., and Walker, R.J., 2016, Highly siderophile elements in Earth, Mars, the Moon, and asteroids, in Harvey, J., and Day, J.M.D., eds., Highly Siderophile and Strongly Chalcophile Elements in High-Temperature Geochemistry and Cosmochemistry: Mineralogical Society of America Reviews in Mineralogy & Geochemistry 81, p. 161–238, <https://doi.org/10.1515/9781501502095-006>.
- Dijkstra, A.H., Sergeev, D.S., Spandler, C., Pettke, T., Meisel, T., and Cawood, P.A., 2010, Highly refractory peridotites on Macquarie Island and the case for anciently depleted domains in the Earth’s mantle: Journal of Petrology, v. 51, p. 469–493, <https://doi.org/10.1093/petrology/egp084>.
- Dubosq, R., Gault, B., Hatzoglu, C., Schweiner, K., Vurpillot, F., Rogowitz, A., Rantitsch, G., and Schneider, D.A., 2020, Analysis of nanoscale fluid inclusions in geomaterials by atom probe tomography: Experiments and numerical simulations: Ultramicroscopy, v. 218, <https://doi.org/10.1016/j.ultramicro.2020.113092>.
- Evans, B.W., 2004, The serpentinite multisystem revisited: Chrysotile is metastable: International Geology Review, v. 46, p. 479–506, <https://doi.org/10.2747/0020-6814.46.6.479>.
- Foustoukos, D.I., 2019, Hydrothermal oxidation of Os: Geochimica et Cosmochimica Acta, v. 255, p. 237–246, <https://doi.org/10.1016/j.gca.2019.04.019>.
- Foustoukos, D.I., Bizimis, M., Frisby, C., and Shirey, S.B., 2015, Redox controls on Ni-Fe-PGE mineralization and Re/Os fractionation during serpentinization of abyssal peridotite: Geochimica et Cosmochimica Acta, v. 150, p. 11–25, <https://doi.org/10.1016/j.gca.2014.11.025>.
- Garuti, G., Zaccarini, F., Proenza, J.A., Thalhammer, O.A.R., and Angeli, N., 2012, Platinum-group minerals in chromitites of the Niquelândia layered intrusion (Central Goiás, Brazil): Their magmatic origin and low-temperature reworking during serpentinization and lateritic weathering: Minerals (Basel), v. 2, p. 365–384, <https://doi.org/10.3390/min2040365>.
- Gorman, J.K., Penniston-Dorland, S.C., Marschall, H.R., and Walker, R.J., 2019, The roles of mechanical mixing and fluid transport in the formation of reaction zones in subduction-related mélange: Evidence from highly siderophile elements: Chemical Geology, v. 525, p. 96–111, <https://doi.org/10.1016/j.chemgeo.2019.07.004>.
- Jiménez-Franco, A., González-Jiménez, J.M., Roqué, J., Proenza, J.A., Gervilla, F., and Nieto, F., 2020, Nanoscale constraints on the in situ transformation of Ru-Os-Ir sulfides to alloys at low temperature: Ore Geology Reviews, v. 124, <https://doi.org/10.1016/j.oregeorev.2020.103640>.
- Keays, R.R., Holwell, D.A., and Prichard, H.M., 2021, Platinum mineralisation in the Owendale Uralian-Alaskan-type complex, New South Wales, Australia: The effects of serpentinization on Cu-PGE-Ni sulphides: Ore Geology Reviews, v. 130, <https://doi.org/10.1016/j.oregeorev.2020.103928>.
- Lawley, C.J.M., Petts, D.C., Jackson, S.E., Zagorevski, A., Pearson, D.G., Kjarsgaard, B.A., Savard, D., and Tschirhart, V., 2020, Precious metal mobility during serpentinization and breakdown of base metal sulphide: Lithos, v. 354–355, <https://doi.org/10.1016/j.lithos.2019.105278>.
- Luguet, A., and Pearson, D.G., 2019, Dating mantle peridotites using Re-Os isotopes: The complex message from whole rocks, base metal sulfides, and platinum group minerals: American Mineralogist, v. 104, p. 165–189, <https://doi.org/10.2138/am-2019-6557>.
- Luguet, A., and Reisberg, L., 2016, Highly siderophile element and <sup>187</sup>Os signatures in non-cratonic basalt-hosted peridotite xenoliths: Unravelling the origin and evolution of the post-Archean lithospheric mantle, in Harvey, J., and Day, J.M.D., eds., Highly Siderophile and Strongly Chalcophile Elements in High-Temperature Geochemistry and Cosmochemistry: Mineralogical Society of America Reviews in Mineralogy & Geochemistry 81, p. 305–368, <https://doi.org/10.1515/9781501502095-008>.
- Matsumoto, A., Matsuno, K., Chiwata, N., Kuwano, N., and Oki, K., 1996, In-situ TEM observation of phase transformation processes in Cu<sub>2</sub>Pt with a long-period superstructure: Journal of Electron Microscopy, v. 45, p. 442–447, <https://doi.org/10.1093/oxfordjournals.jmicro.a023463>.
- McDonough, W.F., and Sun, S.-s., 1995, The composition of the Earth: Chemical Geology, v. 120, p. 223–253, [https://doi.org/10.1016/0009-2541\(94\)00140-4](https://doi.org/10.1016/0009-2541(94)00140-4).
- Park, J.W., Hu, Z.C., Gao, S., Campbell, I.H., and Gong, H.J., 2012, Platinum group element abundances in the upper continental crust revisited—New constraints from analyses of Chinese loess: Geochimica et Cosmochimica Acta, v. 93, p. 63–76, <https://doi.org/10.1016/j.gca.2012.06.026>.
- Parman, S.W., Diercks, D.R., Gorman, B.P., and Cooper, R.F., 2015, Atom probe tomography of isoferroplatinum: American Mineralogist, v. 100, p. 852–860, <https://doi.org/10.2138/am-2015-4998>.
- Reddy, S.M., Saxey, D.W., Rickard, W.D.A., Fougereuse, D., Montalvo, S.D., Verberne, R., and van Riessen, A., 2020, Atom probe tomography: Development and application to the geosciences: Geostandards and Geoanalytical Research, v. 44, p. 5–50, <https://doi.org/10.1111/ggr.12313>.
- Rickard, W.D.A., Reddy, S.M., Saxey, D.W., Fougereuse, D., Timms, N.E., Daly, L., Peterman, E., Cavosie, A.J., and Jourdan, F., 2020, Novel applications of FIB-SEM-based ToF-SIMS in atom probe tomography workflows: Microscopy and Microanalysis, v. 26, p. 750–757, <https://doi.org/10.1017/S1431927620000136>.
- Rudnick, R.L., and Walker, R.J., 2009, Interpreting ages from Re-Os isotopes in peridotites: Lithos, v. 112, p. 1083–1095, <https://doi.org/10.1016/j.lithos.2009.04.042>.
- Salter, V.J.M., Stracke, A., 2004, Composition of the depleted mantle. Geochemistry Geophysics Geosystems 5, <https://doi.org/10.1029/2003gc000597>.
- Secchiari, A., Gleissner, P., Li, C.H., Goncharov, A., Milke, R., Becker, H., Bosch, D., and Montanini, A., 2020, Highly siderophile and chalcophile element behaviour in abyssal-type and supra-subduction zone mantle: New insights from the New Caledonia ophiolite: Lithos, v. 354–355, <https://doi.org/10.1016/j.lithos.2019.105338>.
- Sharygin, V.V., and Mikhaiov, I.G., 2022, Tomamaeite Cu<sub>3</sub>Pt in native osmium from river sediments in the Nizhnie Sergi region, Central Urals: Mineralogy (Russia), v. 8, p. 5–14, <https://doi.org/10.35597/2313-545X-2022-8-2-1>.
- Tacchetto, T., Reddy, S.M., Saxey, D.W., Fougereuse, D., Rickard, W.D.A., and Clark, C., 2021, Disorientation control on trace element segregation in fluid-affected low-angle boundaries in olivine: Contributions to Mineralogy and Petrology, v. 176, 59, <https://doi.org/10.1007/s00410-021-01815-3>.
- Wainwright, A.N., Luguet, A., Fonseca, R.O.C., and Pearson, D.G., 2015, Investigating metasomatic effects on the <sup>187</sup>Os isotopic signature: A case study on micrometric base metal sulphides in metasomatised peridotite from the Letlhakane kimberlite (Botswana): Lithos, v. 232, p. 35–48, <https://doi.org/10.1016/j.lithos.2015.06.017>.
- Zaccarini, F., and Garuti, G., 2020, Zoned laurite from the Merensky Reef, Bushveld Complex, South Africa: “Hydrothermal” in origin?: Minerals (Basel), v. 10, 373, <https://doi.org/10.3390/min10040373>.
- Zhang, H.F., 2008, Variation of Re-Os isotopic system during peridotite-melt interaction: Implication for the meaning of Re-Os isotopic age of Cenozoic mantle peridotites from the North China Craton: Acta Petrologica Sinica, v. 24, p. 2457–2467.
- Zhu, Q.M., and Zhu, Y.F., 2019, Platinum-group minerals and Fe-Ni minerals in the Sartohay podiform chromitite (west Junggar, China): Implications for T-pH-fO<sub>2</sub>-fS<sub>2</sub> conditions during hydrothermal alteration: Ore Geology Reviews, v. 112, <https://doi.org/10.1016/j.oregeorev.2019.103020>.

Printed in USA